IEEE Access
Multidisciplinary : Rapid Review : Open Access Journal

Received April 19, 2021, accepted April 21, 2021, date of publication April 26, 2021, date of current version May 4, 2021.

Digital Object Identifier 10.1109/ACCESS.2021.3075429

AI-Powered Terahertz VLSI Testing Technology for Ensuring Hardware Security and Reliability

NAZNIN AKTER[1], MASUDUR R. SIDDIQUEE[1], MICHAEL SHUR[2,3], (Life Fellow, IEEE), AND NEZIH PALA[1], (Senior Member, IEEE)

[1]Department of Electrical and Computer Engineering, Florida International University, Miami, FL 33174, USA
[2]Department of Electrical Computer and Systems Engineering and the Department of Physics, Applied Physics, and Astronomy, Rensselaer Polytechnic Institute, Troy, NY 12180, USA
[3]Electronics of the Future, Inc., Vienna, VA 22181, USA

Corresponding author: Nezih Pala (npala@fiu.edu)

This work was supported in part by the U.S. Air Force Research Laboratory (AFRL) Small Business Technology Transfer (STTR) Program under Contract FA864919PA080.

ABSTRACT Hardware cybersecurity has become a key issue, especially for very large integrated circuits. If counterfeit, forged, or defective ICs present a significant threat to system reliability and security. The growing complexity of digital and mixed-signal systems makes it increasingly challenging yet vital to develop robust methods to assess and confirm the reliability and authenticity of ICs. We introduce a new terahertz testing method for non-destructive and unobtrusive identification of counterfeit, damaged, forged or defective ICs by measuring their response to incident terahertz and sub-terahertz radiation at the circuit pins and analyzing the response using artificial intelligence (AI). These responses create unique signatures for ICs. We generated 2D images by measuring the response on a selected pin of a radio frequency IC (RFIC) scanned by a focused terahertz radiation. By applying the data augmentation processes, we created a secure image data set to train the convolutional neural network (CNN) model. An unsecured image data set representing altered or damaged ICs was generated by modifying the original image data. The trained models identified secure devices with a ∼94% accuracy.

INDEX TERMS Terahertz, hardware cybersecurity, reliability, authentication, deep learning, convolution neural network, artificial intelligence.

I. INTRODUCTION

With their ever-increasing complexity electronic devices and circuits have become more prone to various security threats. Deliberate alterations can be introduced to highly complex integrated circuits (ICs) at the design, fabrication or packaging stages. Unintended materials and device failures can happen due to the effects such as limited lifetime, premature material deterioration, unpredicted external conditions. Finally, legitimate components and systems can be replaced with the counterfeit ones during shipments. Specifically, the growing use of foreign off-the-shelf components makes faked integrated circuits with additional built-in secret components and/or with malicious software implemented in hardware to be an increasing and powerful hardware security threat. Moreover, considering the fast aging of the widely deployed cyberinfrastructure, it is vital to develop preventive measures and response strategies against all hardware security threats to avoid catastrophic and irreversible consequences [1].

Compromised or untrusted ICs can endanger all additional layers of national or international cyber systems and lead to devastating and far-reaching consequences. It is difficult, even unattainable, to ensure full fault detection using conventional AC and DC electrical testing techniques. An additional security issue comes from fake circuits designed to avoid identification by conventional testing techniques [2]. To differentiate the counterfeit, forged, or damaged ICs from the authentic ICs, straightforward, thorough, non-destructive, and ubiquitous inspection and testing methods are needed. Various non-destructive testing methods have been developed by the IC packaging industry since the 1970s [3], [4]. Besides visual inspection, X-ray [5], [6], scanning acoustic microscopy (SAM) [7], [8], infrared

The associate editor coordinating the review of this manuscript and approving it for publication was Derek Abbott.

This work is licensed under a Creative Commons Attribution 4.0 License. For more information, see https://creativecommons.org/licenses/by/4.0/

thermography (IRT) [9], [10], surface acoustic waves (SAW) [11]–[14] and terahertz transmission and reflection imaging [15] have been adopted for the non-destructive testing and inspection methods of IC packaging. Terahertz imaging technology can be an ideal approach for defect detection because several materials have unique spectral fingerprinting characteristics in the terahertz spectral region. Utilizing the advantages provided by terahertz systems it is feasible to perform authentication [16], non-destructive inspection [17]–[21], laser terahertz emission spectroscopy (LTEM) [22], [23] for VLSI testing, terahertz time-domain reflectometry (THz-TDR) [24], terahertz scanning near-field optical microscope (THz-SNOM) and terahertz scanning tunneling microscope (THz-STM) [25], [26], large scale integrated circuit (LSIC) inspection [27], 3D imaging [28]–[30], quality control [31]–[35], airport security [36]–[40], art investigations [41], tomography [29], [42]–[44], biomedical diagnosis and imaging [45]–[47], material characterization [48]–[53], thickness measurements [54], [55], and holography [56], [57].

Although terahertz imaging systems provide a broad spectrum of applications, they suffer from inherent low-resolution imaging, which poses a significant hindrance to draw the attention of the industrial sector to employ terahertz imaging systems as practical tools for advanced very large scale integration (VLSI) circuits (with minimum feature sizes down to 7 nm, 5 nm and even 3 nm) [58], [59]. Instead of using the terahertz imaging technique, a new approach of terahertz testing of monolithic microwave integrated circuits (MMICs) and VLSI circuits is possible by measuring the circuit's DC bias responses at the pins or input/output contacts or leads [60]–[64] and then analyzing these responses with etalon responses [65]–[69]. Minor biasing modifications may also trigger significant changes to the transistor's response, which improves the usefulness of the approach. voltages induced by terahertz or sub-terahertz radiation at the IC terminals can be used as a diagnostic mechanism for defects or deviations from the expected outcome. Such voltages may form specific signatures of defects. This method can also predict the lifetime and reliability following the fault diagnosis and identification process. At low terahertz radiation intensities, the DC voltage will be proportional to the intensity, while at high terahertz radiation intensities, it will likely be proportional to the intensity's square root [70] or saturate [71]. For transistors with defects, such as high leakage currents [72], for instance, this response will be very different. Usually, the transistor gate size specifies the spatial resolution of this defect-detection technique. Additional testing details can be achieved when the impinging terahertz beam is scanned through the circuit [72].

In our work, we have used the terahertz response of ICs as signature data to classify secured and unsecured/faulty ICs. We measured the DC response on a selected pin of a radio frequency integrated circuits (RFIC) while scanning a focused terahertz beam on it to obtain a 2D signature response map. Resolution of our technique is in the nanometer range, even though the radiation wavelength is hundreds of micrometers. By applying data augmentation processes, we have created a secure image data set to train the convolutional neural network (CNN) models. We have also used the data augmentation method by adding randomized noise in the authentic response data and produced randomized response data. We have then divided all response data into two categories: 1) Secure response set and 2) unsecure response set and fed these data sets into our CNN model. We distinguished the classified images with accurate prediction based on the established MATLAB coded CNN data classification process. We have also designed a graphical user interface (GUI) using the MATLAB App Designer for end-users to train CNN with new data and identify ICs easily. The focus of the presented work is to demonstrate a novel terahertz response-based testing method using well developed artificial intelligence (AI) techniques.

The rest of the paper is organized as follows. In the next section, we give a brief overview of the available IC testing methods. Section III focuses on the terahertz based IC response mapping used in this work. The experimental setup using an IMPATT diode and a short review of the convolution neural network (CNN) are presented in Section IV. Section V presents the results and their detailed discussion and classification of the secured and unsecured IC responses.

II. TERAHERTZ, IMPEDANCE-BASED, AND X-RAY IC TESTING

An extensive range of test schemes is currently attainable for detecting and identifying counterfeit parts. These techniques intend to recognize the defects existing in a part or a batch of parts. A counterfeit IC part may comprise one or more diverse types of anomalies and deviations from an authenticate component's functionality. These anomalies could be physical (i.e., related to the leads, package), electrical (e.g., degradation in its performance or a change in its specifications), or intentional (insertion of hardware trojan or backdoor software). In the following subsection, we will briefly describe terahertz, impedance, and X-ray imaging-based IC testing.

A. TERAHERTZ SCANNING SYSTEMS

The packaging materials of authentic and counterfeit ICs might differ. Based on the package materials properties, the effective refractive index and amplitude extinction coefficient vary significantly. The intensity and time delay of the traversed terahertz pulse through the packaging of both authentic and counterfeit or defective ICs can be recorded and compared by utilizing the terahertz time domain spectroscopy (THz-TDS) systems [15]. Generally, the traversed terahertz pulses from the counterfeit ICs show different time delays and attenuations than the authentic ICs, which results from the different effective refractive index and the amplitude extinction coefficient value. A different material profile for each ICs can be deduced from the measured time delays and attenuations using the terahertz reflected setup [15]. It is also

possible to measure the thickness of the hidden layers in the packaged ICs through the recorded terahertz pulses time delays.

B. IMPEDANCE BASED IC TESTING

ICs offer unique frequency-dependent scattering responses to an input RF signal for each pin [73]. These scattered frequency-dependent responses can be used to represent a distinctive signature of an individual IC with high repeatability. The underlying physics is linked to the origin of the input impedance of external nodes. The impedance is a function of frequency and signal path within a circuit due to the complex mutual coupling effects at RF and higher frequencies. The information on the IC device packaging is essential to measure these frequencies and path-dependent signatures. This impedance-based measurement technique is repeatable, passive, and non-destructive, which can distinguish the counterfeit or forged ICs.

C. X-RAY IMAGING FOR IC TESTING

Ptychographic X-ray laminography is capable of non-destructively extracting the 3D design of a modern microprocessor [74]. This process can further speed up by starting with more information about the chip. This method of non-destructive reverse engineering of electronic chips could check that chip manufacturing was done according to the original design. X-ray ptychography can be used in unthinned integrated circuits up to 240 μm in thickness to image circuit features at sub-20-nm resolution, allowing one to image chips with no restrictions fragility and heat transport imposed by thinning, thereby retaining the possibility for electrical testing [75].

III. TERAHERTZ RESPONSE BASED IC TESTING

Our proposed method is based on the fact that a modern field-effect transistor (FET) with a sufficiently short channel can serve as a terahertz detector. This detection process has a subwavelength resolution. The impinging terahertz radiation on a transistor couples through the contacts or interconnects and excites the overdamped or resonant plasma waves, i.e., the waves of the electron density in the device channel. The rectified response due to the transistor nonlinearities results in an induced DC voltage on the I/O pins. A lock-in amplifier is used to measure and record the frequency modulated response. The IC can be placed on a nano-stage, and the induced DC response can be scanned by moving the IC in 3D (x, y, and z) under the impinging terahertz radiation. The resulting spatial dependence of the response depends on the collective response of all the FETs in the IC and forms a unique signature that could be used to differentiate genuine/healthy ICs from forged/defective ones. Feasibility of this technique has been experimentally proven in [66] and [76]. The method described in these references, although successful, is not suitable for high throughput testing of complex ICs. Our work here more specifically targets at extending the previous work by adding automated scanning

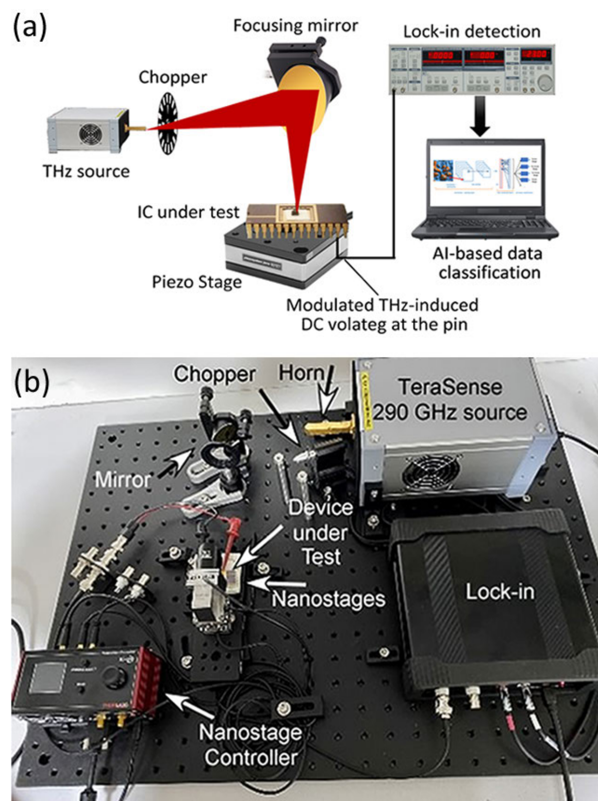

FIGURE 1. (a) Schematic presentation of the terahertz scanning setup for generating spatial terahertz response map for AI based image processing. (b) Picture of the experimental setup.

and AI analysis to demonstrate a proof-of-concept platform for fast and accurate IC testing. Fig. 1(a) shows the schematic description of the terahertz IC testing method used in this study.

A significant advantage of this new non-invasive and non-destructive technique compared to other radiation enhanced testing methods is that this approach does not affect the device operation and could work with no bias or under bias. In contrast to the conventional terahertz imaging, this technique can use the intensity, polarization, frequency, and bias dependences of the terahertz response at the VLSI or MMIC pins for a more detailed IC response. It can also find applications as a testing technique for Si and compound semiconductor devices and circuits for defect identification, reliability prediction, and fabrication process optimization. It should be noted that the spatial resolution of our technique is aperture (typically gate of the transistors) limited and therefore can reach down to nanometer range, even though the radiation wavelength is hundreds of micrometers. Such resolution has been demonstrated in previous papers of ours [77] and others [25]–[27].

IV. EXPERIMENTAL METHODS

A. TERAHERTZ IC SCANNING SYSTEMS

For the experimental data acquisition, we used a fixed frequency IMPATT diode-based terahertz source operating

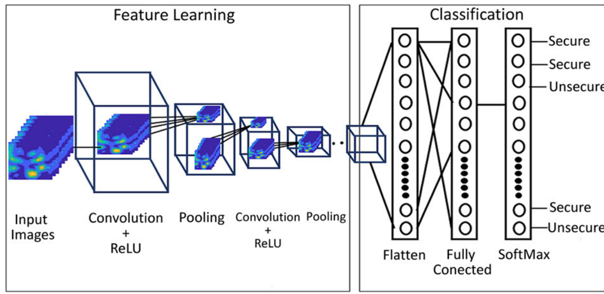

FIGURE 2. Basic model of Convolution Neural Network (CNN).

at 0.289 THz with an 8.5 mW output power and with 26dB gain detachable horn antenna. This setup is shown in Fig. 1(b).

The samples that were wire-bonded on the chip carriers placed on three-axis nano-stages controlled with a computer connected KIM101 controller and had the steps down to 5 μm. The Stanford Research SR830 DSP lock-in-amplifier measured the response with an optical chopper. Custom LabView codes performed all the equipment control and data acquisition.

B. DEEP LEARNING – CONVOLUTION NEURAL NETWORK (CNN)

We have implemented the standard Convolutional Neural Network (CNN) offered by the deep network designer app from MATLAB in our study. To design the CNN model, we selected one image input layer, three convolution 2D layers, two batch normalization layers, three rectified linear unit (ReLU) layers, two max-pooling layers, one fully connected layer, one SoftMax, and one classification layer. CNN is the best method for data classification in deep learning neural networks inspired by the visual cortex layout. Fig. 2 shows the basic convolutional neural network model that we have used for image classification. The whole CNN consists of two categories: i) Feature learning and ii) classification. The feature learning section consists of convolutional layers, ReLU layers, and pooling layers, and the classification section consists of fully connected layers and SoftMax activation function. The convolution layer usually consists of convolution operation (also known as a convolution filter or kernel), activation function, feature map, or an activation map. The convolution operation is intended to extract high-level features from the input image, such as edges. For CNN to capture the low-level features such as edges, color, and gradient orientation, only one convolution layer is required. The framework adapts to the high-level characteristics with added layers and forms a model with a detailed understanding of the dataset's images. For the activation function, CNN uses ReLU sigmoid, and tanh function based on the application. Among these, to increase nonlinearity in neural networks, especially in CNNs, ReLU is the most used activation function. The number of generated feature maps is the same as the number of the convolution filters, and the result of the

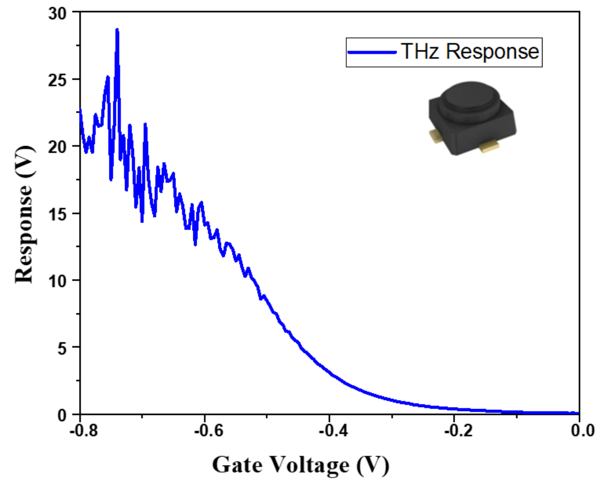

FIGURE 3. Measured terahertz response on a selected pin (Inset: CE3520K3 IC).

convoluted feature map is smaller than the original image. In order to get different results, a feature detector can be set with different values, such as sharpening and focusing on an image or blurring an image.

The pooling layer's primary function is to reduce the convoluted feature's spatial size, which decreases the computational power needed to process the data. After applying the pooling layer to the feature map, the pooled feature map is formed. Pooling is carried out using either the Max Pooling or the Mean Pooling forms. Max Pooling returns the maximum value, whereas the Mean Pooling returns the average of all the image portion values. The feature learning portion's fundamental objective is to extract the features and preserve them in a feature map while retaining the pixels' spatial relationship. All the inputs from other layers will be flattened into a vector and render the classes through voting in a fully connected layer. This layer using the SoftMax activation operator will transform the output into the desired number of classes by the network; in our case, the classes are secure and insecure. The CNN model trains the images using forward and backward propagation for a consecutive number of epochs.

V. RESULTS AND DISCUSSIONS

We measured the terahertz response of super-low noise and high gain amplifier integrated circuits (CE3520K3). Fig. 3 shows the measured DC voltage response on a selected pin of the device under large area unfocused terahertz exposure at 0.289 THz while Fig. 4 shows the measured response for scanning a tightly focused terahertz beam over the chip. This response can generate a terahertz -response signature for an IC. For the classification study, 2D measurements scans have been recorded using a 3D nano-stage. The focused terahertz beam was scanned over the IC and moved 25 steps in x and y directions. We have acquired six data sets shown in Fig. 4 through the scan of the sample under terahertz radiation. The response measured at the selected in of the

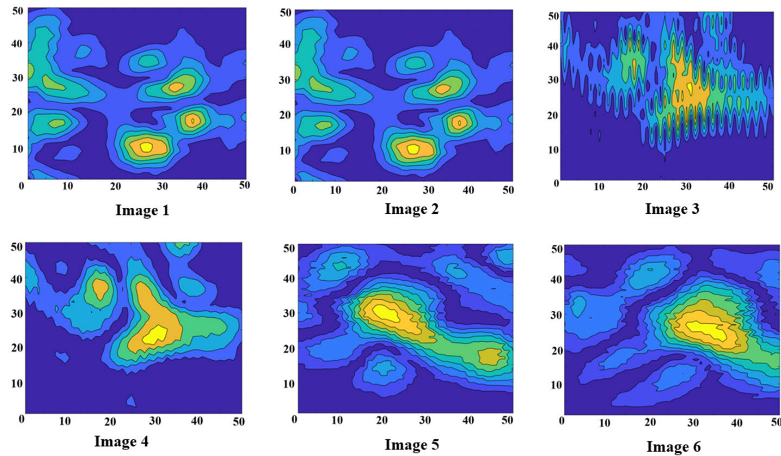

FIGURE 4. Measured position dependent DC response at a selected pin of the tested IC while a 0.289 THz beam is scanned in 2D.

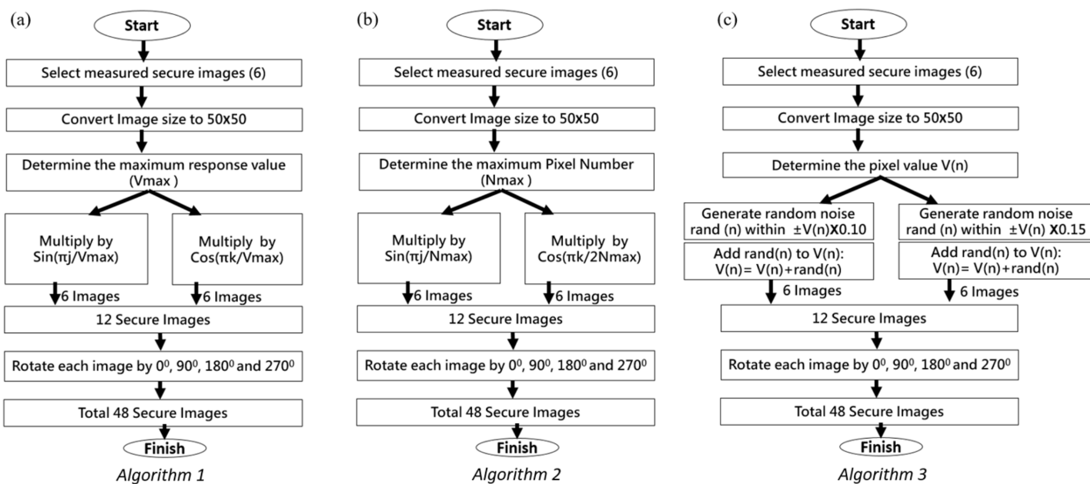

FIGURE 5. Algorithms used for secure image data augmentation.

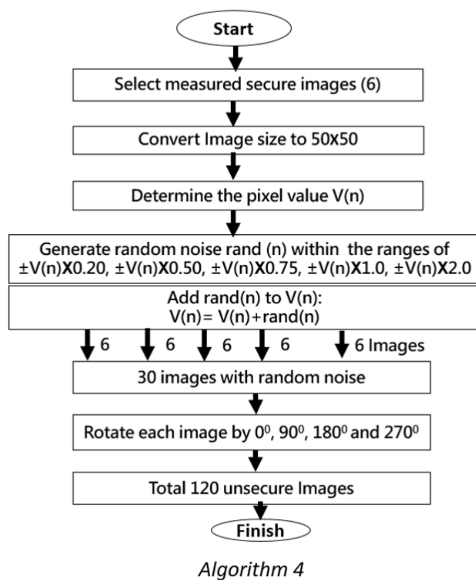

FIGURE 6. Algorithms The algorithm used to obtain unsecure data sets for training and testing.

same device under the same biasing conditions. The image 1 and image 2 are results of the two subsequent scans. These two images illustrate the reproducibility of our technique. The height of the device holder was then changed for the next scans resulting in images 3 to 6. The differences in the measured scans 2 to 6 are due to the different focal point in the vertical direction. This process allowed us to obtain secure images accounting for different vertical positions of the scanning beam. Measuring the response of different pins would have different 2D response map for each pin which could also be used for classification. Such measurements would be especially useful for complicated VLSI with a large number of transistors. We have performed preliminary measurements of the different pin response for Intel^{TM} i7 microprocessor. A generalization of our AI approach for such complex VLSI is in progress and will be reported elsewhere. The measured data smoothened to 50 $\times$ 50-pixel data sets are considered as the original or secure images. The similarity of the data obtained by the subsequent scans, except for the set of the images 3 and 4, clearly shows the repeatability of the

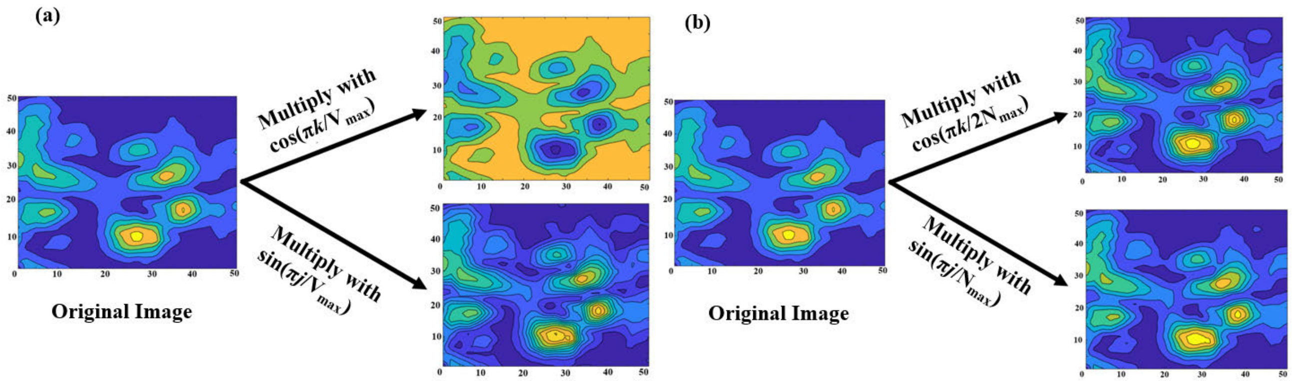

FIGURE 7. Image generated by multiplying the original image set with (a) $\sin(\pi j/V_{\max})$ and $\cos(\pi k/V_{\max})$, and (b) $\sin(\pi j/N_{\max})$ and $\cos(\pi k/2N_{\max})$.

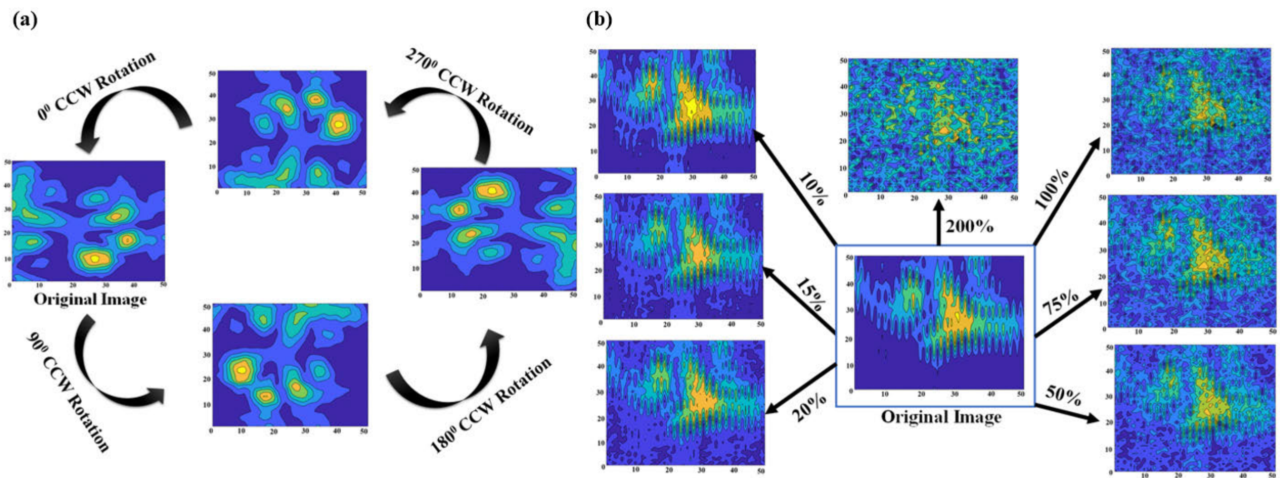

FIGURE 8. (a) 0°,90°, 180°- and 270°-degree counter-clockwise rotational images, and (b) randomized image generation from its original image through 10%, 15%, 20%, 50%, 75%, 100%, and 200% randomized image sets.

measurements. The apparent distortion of the data in image 3 was attributed to a measurement setup malfunction. Nevertheless, we used in our data analysis to augment the data for AI training. We have considered four algorithms to create altered images data set using the data augmentation (Fig. 5 and 6).

Algorithm 1: We have multiplied the six images data set first by $\sin(\pi j/V_{\max})$ and then by $\cos(\pi k/V_{\max})$, where $V_{\max}$ is the maximum measured response value and the value of *j, k* is in the range from 1 to $N_{\max}$that is the maximum number of pixels in a row/column (50 in the present case). Fig. 5(a) shows the sample images generated using the trigonometric function depending on the $V_{\max}$ to increase the data set number. We further rotated each image by 90°, 180°, and 270°. Hence, this algorithm has produced 48 total new images.

Algorithm 2: We have multiplied the same six initial image data set by $\sin(\pi j/N_{\max})$ and by $\cos(\pi k/2N_{\max})$, where $N_{\max}$ is the maximum number of pixels in a row/column (50) and the value of *j, k* is in the range from 1 to $N_{\max}$. Fig. 5(b) shows the image generation using this method. All images were then rotated by 90°, 180°, and 270° to obtain 48 images (Fig 5(b).

Algorithm 3: This data augmentation algorithm was adding random noise with a maximum amplitude of 10%, 15% of the measured response value to the measured data set. To generate 10% (15%) random data, we used each pixel value of the original image. We added a random value in between ± 10% (± 15%) of the original image's pixel value to create the 10% randomized images data set. This approach inherently assumes that variations up to 15% are acceptable in device geometries and characteristics are acceptable. The rate can be changed for specific devices/process fabrication foundries to train the AI for improved accuracy. All images then were rotated by 90°, 180° and 270° to obtain 48 more images. Fig. 5(c) shows the image generation using this method.

Algorithm 4: Like the previous one, we added random noise with the maximum amplitude of 20%, 50%, 75%, 100%, and 200% of the measured response value to the measured data set (Fig. 6). All images then were rotated by 90°, 180° and 270° to have the final set of altered images.

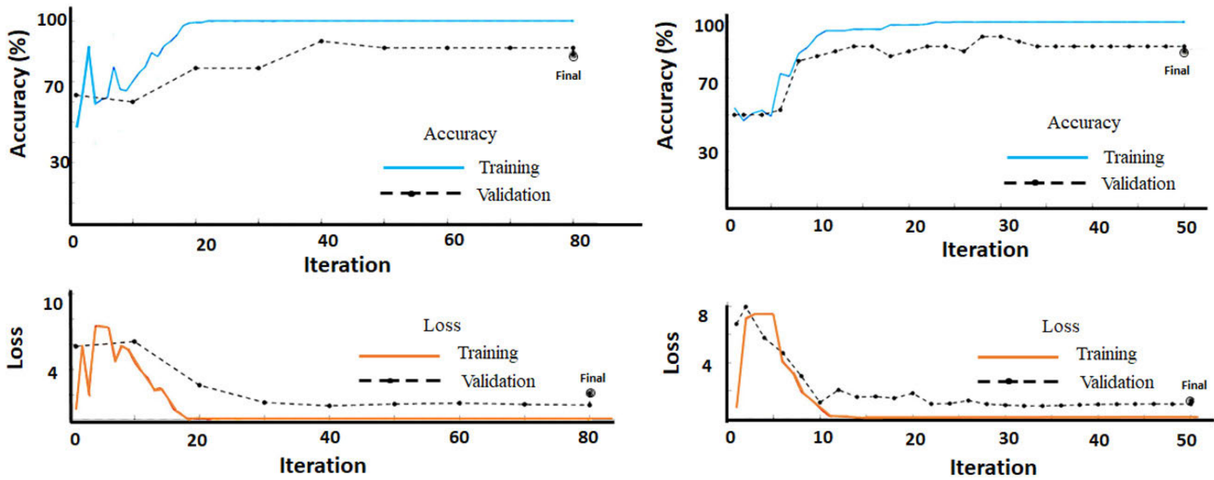

FIGURE 9. Our CNN model training progress chart for (a) approach 1, and (b) approach 2.

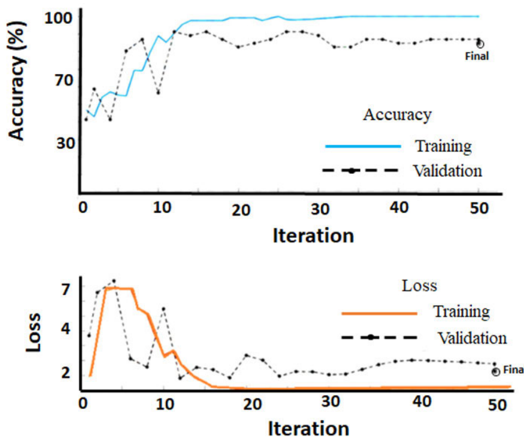

FIGURE 10. CNN model training progress chart for approach 3.

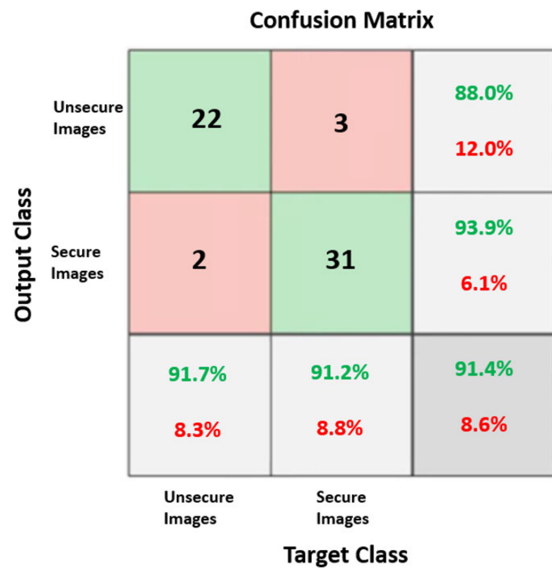

FIGURE 11. Confusion matrix.

We have classified the images as secure and unsecured as shown in Fig. 7 (a) & (b) and Fig. 8 (a) & (b) respectively. We have categorized all images generated from Algorithms 1-3 as secure image data sets, while images generated by Algorithm 4 have been considered unsecure image data sets.

We have separated 80% of the data sets into secure and unsecure categories for CNN training and the remaining 20% for testing the trained CNN. All the training samples pass through the learning algorithm concurrently in one epoch before the weights are updated. All the weights are updated for sequential training after each training vector is passed sequentially through the training algorithm. For a small number of epochs in the training algorithms, the training is poor, and underfitting effects happen. If the network is trained too much, it will memorize the desired outputs for the training inputs. Considering how important the number of epochs is, we have set the maximum epoch value as initially 80 and 50. The initial learning rate of our model is 10-4. Validation frequency, which is also an important parameter defining the number of iterations between evaluations of validation metrics, was set to 2 for our model set. To validate our CNN model accuracy, we have used three different approaches.

Approach 1: In the first approach, we have considered the original images, their rotations, and the images obtained using Algorithm 3 described above, resulting in 72 images for the secure images set. For the unsecure images set, we have considered the 120 images obtained using Algorithm 4. After using 80% of each set for training the CNN model, we tested it using the remaining 20%. The model yielded 83.33 % training accuracy and an 87.12 % testing accuracy, as shown in Fig. 9(a).

Approach 2: We took the original images, and their rotational variants, and the images obtained using Algorithms 1 and 3, resulting in 120 images for the secure images set. The same data set yielded by the previous approach was used for the unsecure images. We trained the CNN model using 80% of each data set and tested using 20%. This

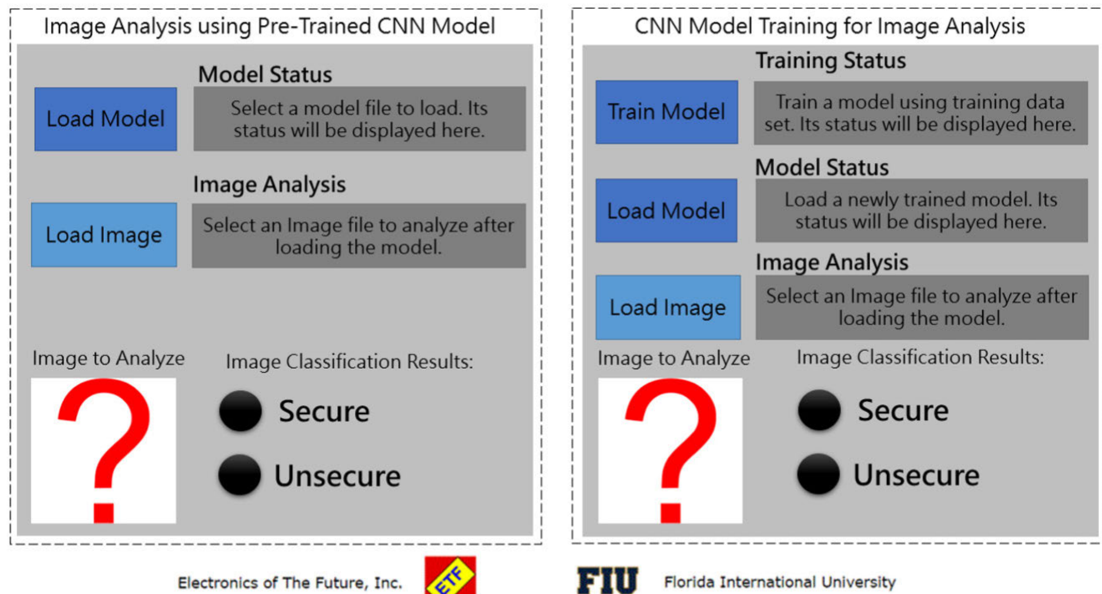

FIGURE 12. Screenshot of the AI-Powered THz IC testing application user interface.

approach achieved 84.21 % training accuracy and a 93.75 % testing accuracy as shown in Fig. 9(b).

Approach 3: In the third approach, we used the original images, and their rotational variants, and the images obtained by using Algorithms 1, 2, and 3 to form a secure date set of 168 images. For the unsecure data set, we used the same data set of 120 images as in the previous approach. The tests performed using 20% of the sets resulted in 84.78 % training accuracy and 86.21 % testing accuracy, as shown in Fig. 10.

For the first approach, the max epoch was set to 80. For the second and third approaches, the max epoch was set to 50. For the first approach, only one convolution layer was used, while for the second and third approaches, three convolution layers were used to avoid the data overfitting issue and to increase the CNN model performance. Based on our model, we can conclude that the number of samples significantly impacts attaining a higher accuracy rate. Suppose both the classification has the same amount of sample images. In that case, the model has a 94% chance to correctly classify images that are very similar to the trained data, which is a pretty good accuracy rate for image processing and training.

A confusion matrix is a method to summarize the predicted results of a classification algorithm's performance. Using the Approach 3, we processed 288 images (168 secure images and 120 unsecure images) out of which, 80% were used for training, and 20% were used for testing. We have used the testing dataset (33 secure and 25 unsecure, totaling 58 images) to plot the confusion matrix shown in Fig. 11. In the figure, the first two diagonal cells (green shaded) show the number of the correct classifications by the trained network.

Row1-Column1 shows that 22 unsecure images (out of 25 total) were correctly classified as unsecure images, and Row2-Column2 shows that 31 images (out of 33 total) were correctly classified as secure. Row1-Column2 shows that 3 of the unsecure images were incorrectly classified as secure, which corresponds to 5.2% false-negative of all 58 images in the data. Similarly, Row2-Column1 shows 2 of the secure images were incorrectly classified as unsecure, which corresponds to 3.4% false-positive of all data. Row3-Column1 shows that out of 24 unsecure predictions, 91.7% were correct, and 8.3% were wrong. Row3-Column2 shows that out of 34 secure predictions, 91.2% were correct, and 8.8% were wrong. Row1-Column3 shows that out of 25 unsecure predictions, 88.0% were correct, and 12.0% were wrong. Row2-Column3 shows that out of 33 secure predictions, 93.9% were correct, and 6.1% were wrong. Row3-Column3 represents the overall predictions where 91.4% were correct, and 8.6% were wrong. Based on these results, we can claim that our proposed approach can accurately classify the image type although we have used a small number of image datasets and a simple CNN model. The accuracy can be further improved using a significant number of datasets and optimized CNN.

We have also developed a MATLAB application, and a standalone application with a graphical user interface (GUI) using the MATLAB App Designer, as shown in Fig. 12. The GUI-based application allows end users to input known secure and unsecure images for training as well as unknown images for identification effortlessly. It makes the presented system easy to use with minimal training.

VI. CONCLUSION

In conclusion, we successfully demonstrated a novel terahertz AI testing method for non-destructive and unobtrusive identification and classification of genuine ICs and counterfeit, damaged, or forged ICs. Our applied approach is based on measuring the IC response to terahertz and sub-terahertz radiation at the circuit pins. Measuring at a larger number of pins under different frequencies and polarizations of terahertz radiation can produce more complex terahertz response signatures, which would result in higher classification accuracy. Our proposed approach does not affect the IC operation and could provide detailed IC signatures. We explained the classification process between the secure and unsecure IC images using the convolution neural network with ∼86 to 94% accuracy and its graphical user interface. This accuracy level can be further improved by using transfer learning to suppress any data overfitting issues. Terahertz signatures of the individual ICs can be generated by applying different measurement processes under different polarization, frequency, and depth of focuses.

REFERENCES

[1] A. Gattiker, P. Nigh, and R. Aitken, "An overview of integrated circuit testing methods," in *Proc. ASM Int. Microelectron. Failure Anal.*, 2019, pp. 634–642.

[2] D. Hély, K. Rosenfeld, and R. Karri, "Security challenges during VLSI test," in *Proc. IEEE 9th Int. New Circuits Syst. Conf. (NEWCAS)*, Jun. 2011, pp. 486–489.

[3] R. J. Ross, *Microelectronics Failure Analysis: Desk Reference*. 6th ed. Materials Park, OH, USA: ASM International, 2011.

[4] P. Aryan, S. Sampath, and H. Sohn, "An overview of non-destructive testing methods for integrated circuit packaging inspection," *Sensors*, vol. 18, no. 7, Jun. 2018, Art. no. 1981.

[5] S. M. Rooks, B. Benhabib, and K. C. Smith, "Development of an inspection process for ball-grid-array technology using scanned-beam X-ray laminography," *IEEE Trans. Compon., Package., Manuf. Technol., A*, vol. 18, no. 4, pp. 851–861, Dec. 1995.

[6] Y. J. Roh, K. W. Ko, H. Cho, H. C. Kim, H. Joo, and S. K. Kim, "Inspection of ball grid array (BGA) solder joints using X-ray cross-sectional images," in *Proc. 8th Mach. Vis. Syst. Inspection Metrol.*, vol. 3836, Aug. 1999, pp. 168–178.

[7] J. E. Semmens and L. W. Kessler, "Further investigation into the use of acoustic micro imaging for analyzing flip chip integrity and failure modes," in *Proc. Int. Conf. Multichip Modules*, 1997, pp. 165–169.

[8] J. E. Semmens and L. W. Kessler, "Characterization of flip chip interconnect failure modes using high frequency acoustic micro imaging with correlative analysis," in *Proc. 35th Annu. IEEE Int. Rel. Phys. Symp.*, Apr. 1997, pp. 141–148.

[9] O. Breitenstein, J. P. Rakotoniaina, F. Altmann, J. Schulz, and G. Linse, "Fault localization and functional testing of ICs by lock-in thermography," in *Proc. Conf. 28th Int. Symp. Test. Failure Anal. (ISTFA)*, Oct. 2002, pp. 29–38.

[10] T. C. Chai, B. S. Wongi, W. M. Bai, A. Trigg, and Y. K. Lain, "A novel defect detection technique using active transient thermography for high density package and interconnections," in *Proc. 53rd Electron. Compon. Technol. Conf.*, 2003, pp. 920–925.

[11] S. Liu and I. C. Ume, "Vibration analysis based modeling and defect recognition for flip-chip solder-joint inspection," *J. Electron. Packag.*, vol. 124, no. 3, pp. 221–226, Jul. 2002.

[12] L. Su, T. Shi, Z. Liu, H. Zhou, L. Du, and G. Liao, "Nondestructive diagnosis of flip chips based on vibration analysis using PCA-RBF," *Mech. Syst. Signal Process.*, vol. 85, pp. 849–856, Feb. 2017.

[13] S. Liu, D. Erdahl, C. Ume, and A. Achari, "A novel method and device for solder joint quality inspection by using laser ultrasound," in *Proc. 50th Electron. Compon. Technol. Conf.*, 2000, pp. 408–415.

[14] D. M. Pepper, G. J. Dunning, M. P. Chiao, T. R. O'Meara, and P. V. Mitchell, "Inspection of flip-chip epoxy underfill in microelectronic assemblies using compensated laser-based ultrasonic receivers," in *Review of Progress in Quantitative Nondestructive Evaluation*. New York, NY, USA: Springer, 1998, pp. 1943–1950.

[15] K. Ahi, S. Shahbazmohamadi, and N. Asadizanjani, "Quality control and authentication of packaged integrated circuits using enhanced-spatial-resolution terahertz time-domain spectroscopy and imaging," *Opt. Lasers Eng.*, vol. 104, pp. 274–284, May 2018.

[16] K. Ahi, N. Asadizanjani, S. Shahbazmohamadi, M. Tehranipoor, and M. Anwar, "Terahertz characterization of electronic components and comparison of terahertz imaging with X-ray imaging techniques," *THz Phys., Devices, Syst., Adv. Appl. Ind. Defense*, vol. 9483, May 2015, Art. no. 94830K.

[17] I. S. Gregory, W. R. Tribe, C. Baker, B. E. Cole, M. J. Evans, L. Spencer, M. Pepper, and M. Missous, "Continuous-wave terahertz system with a 60 dB dynamic range," *Appl. Phys. Lett.*, vol. 86, no. 20, May 2005, Art. no. 204104.

[18] M. Wienold, T. Hagelschuer, N. Rothbart, L. Schrottke, K. Biermann, H. T. Grahn, and H.-W. Hübers, "Real-time terahertz imaging through self-mixing in a quantum-cascade laser," *Appl. Phys. Lett.*, vol. 109, no. 1, Jul. 2016, Art. no. 011102.

[19] E. V. Yakovlev, K. I. Zaytsev, I. N. Dolganova, and S. O. Yurchenko, "Non-destructive evaluation of polymer composite materials at the manufacturing stage using terahertz pulsed spectroscopy," *IEEE Trans. THz Sci. Technol.*, vol. 5, no. 5, pp. 810–816, Sep. 2015.

[20] M. Kato, S. R. Tripathi, K. Murate, K. Imayama, and K. Kawase, "Non-destructive drug inspection in covering materials using a terahertz spectral imaging system with injection-seeded terahertz parametric generation and detection," *Opt. Exp.*, vol. 24, no. 6, pp. 6425–6432, Mar. 2016.

[21] P. Lopato and T. Chady, "Terahertz detection and identification of defects in layered polymer composites and composite coatings," *Nondestruct. Test. Eval.*, vol. 28, no. 1, pp. 28–43, Mar. 2013.

[22] M. Yamashita, K. Kawase, C. Otani, T. Kiwa, and M. Tonouchi, "Imaging of large-scale integrated circuits using laser-terahertz emission microscopy," *Opt. Exp.*, vol. 13, no. 1, pp. 115–120, 2005.

[23] M. Yamashita, T. Kiwa, M. Tonouchi, K. Nikawa, C. Otani, and K. Kawase, "Laser terahertz emission microscope for inspecting electrical failures in integrated circuits," in *Proc. Int. Meeting for Future Electron Devices*, 2004, pp. 29–30.

[24] M. Nagel and H. Kurz, "Terahertz imaging: Terahertz reflectometry images faults in silicon chips," *Laser Focus World*, vol. 47, no. 11, p. 61, 2011.

[25] T. L. Cocker, D. Peller, M. A. Huber, F. Mooshammer, M. Plankl, F. Sandner, L. Viti, M. S. Vitiello, J. Repp, and R. Huber, "Terahertz microscopy down to the atomic scale," in *Proc. 43rd Int. Conf. Infr., Millim., THz Waves (IRMMW-THz)*, Sep. 2018, pp. 1–4.

[26] T. L. Cocker, D. Peller, P. Yu, J. Repp, M. A. Huber, F. Mooshammer, M. Plankl, L. Viti, F. Sandner, L. Z. Kastner, and M. S. Vitiello, "Sub-cycle terahertz microscopy down to the atomic scale," in *Proc. Workshop Adv. Scanning Probe Microsc. (ASPM)*, 2018. Accessed: Jan 18, 2021. [Online]. Available: http://aspm.kr/wp-content/uploads/L_Cocker.Tyler_.pdf

[27] K. Kawase, "Terahertz imaging for drug detection and large-scale integrated circuit inspection," *Opt. Photon. News*, vol. 15, no. 10, pp. 34–39, Oct. 2004.

[28] V. P. Wallace, E. MacPherson, J. A. Zeitler, and C. Reid, "Three-dimensional imaging of optically opaque materials using nonionizing terahertz radiation," *J. Opt. Soc. Amer. A, Opt. Image Sci.*, vol. 25, no. 12, pp. 3120–3133, 2008.

[29] J. B. Perraud, A. F. Obaton, J. Bou-Sleiman, B. Recur, H. Balacey, F. Darracq, J.-P. Guillet, and P. Mounaix, "Terahertz imaging and tomography as efficient instruments for testing polymer additive manufacturing objects," *Appl. Opt.*, vol. 55, no. 13, pp. 3462–3467, 2016.

[30] H. Balacey, B. Recur, J.-B. Perraud, J. B. Sleiman, J.-P. Guillet, and P. Mounaix, "Advanced processing sequence for 3-D THz imaging," *IEEE Trans. THz Sci. Technol.*, vol. 6, no. 2, pp. 191–198, Mar. 2016.

[31] H. Zhong, N. Karpowicz, J. Xu, Y. Deng, W. Ussery, M. Shur, and X.-C. Zhang, "Inspection of space shuttle insulation foam defects using a 0.2 THz Gunn diode oscillator," in *Infr. Millim. Waves, Conf. Dig. Joint 29th Int. Conf., 12th Int. Conf. THz Electron.*, 2004, pp. 753–754.

[32] R. I. Stantchev, B. Sun, S. M. Hornett, P. A. Hobson, G. M. Gibson, M. J. Padgett, and E. Hendry, "Noninvasive, near-field terahertz imaging of hidden objects using a single-pixel detector," *Sci. Adv.*, vol. 2, no. 6, Jun. 2016, Art. no. e1600190.

[33] F. Rutz, M. Koch, S. Khare, M. Moneke, H. Richter, and U. Ewert, "Terahertz quality control of polymeric products," *Int. J. Infr. Millim. Waves*, vol. 27, no. 4, pp. 547–556, Feb. 2007.
[34] Z. Popovic and E. N. Grossman, "THz metrology and instrumentation," *IEEE Trans. THz Sci. Technol.*, vol. 1, no. 1, pp. 133–144, Sep. 2011.
[35] L. Angrisani, G. Cavallo, A. Liccardo, G. P. Papari, and A. Andreone, "THz measurement systems," in *New Trends and Developments in Metrology*. London, U.K.: InTech, 2016, pp. 21–48.
[36] V. A. Trofimov, V. V. Trofimov, I. E. Kuchik, and I. L. Shestakov, "New algorithm for detection of dangerous objects hidden on a human body using passive THz camera," in *Proc. 9th Millimetre Wave THz Sensors Technol.*, vol. 9993, Oct. 2016, Art. no. 999305.
[37] I. N. Dolganova, K. I. Zaytsev, A. A. Metelkina, V. E. Karasik, and S. O. Yurchenko, "A hybrid continuous-wave terahertz imaging system," *Rev. Sci. Instrum.*, vol. 86, no. 11, Nov. 2015, Art. no. 113704.
[38] M. Kowalski and M. Kastek, "Comparative studies of passive imaging in terahertz and mid-wavelength infrared ranges for object detection," *IEEE Trans. Inf. Forensics Security*, vol. 11, no. 9, pp. 2028–2035, Sep. 2016.
[39] M. Kowalski, M. Kastek, M. Walczakowski, N. Palka, and M. Szustakowski, "Passive imaging of concealed objects in terahertz and long-wavelength infrared," *Appl. Opt.*, vol. 54, no. 13, pp. 3826–3833, May 2015.
[40] E. Grossman, C. Dietlein, J. Ala-Laurinaho, M. Leivo, L. Gronberg, M. Gronholm, P. Lappalainen, A. Rautiainen, A. Tamminen, and A. Luukanen, "Passive terahertz camera for standoff security screening," *Appl. Opt.*, vol. 49, no. 19, pp. E106–E120, 2010.
[41] H. Zhang, S. Sfarra, K. Saluja, J. Peeters, J. Fleuret, Y. Duan, H. Fernandes, N. Avdelidis, C. Ibarra-Castanedo, and X. Maldague, "Non-destructive investigation of paintings on canvas by continuous wave terahertz imaging and flash thermography," *J. Nondestruct. Eval.*, vol. 36, no. 2, p. 34, Apr. 2017.
[42] N. Rothbart, H. Richter, M. Wienold, L. Schrottke, H. T. Grahn, and H.-W. Hubers, "Fast 2-D and 3-D terahertz imaging with a quantum-cascade laser and a scanning mirror," *IEEE Trans. THz Sci. Technol.*, vol. 3, no. 5, pp. 617–624, Sep. 2013.
[43] M. W. Ayech and D. Ziou, "Terahertz image segmentation using k-means clustering based on weighted feature learning and random pixel sampling," *Neurocomputing*, vol. 175, pp. 243–264, Jan. 2016.
[44] B. Ferguson, S. Wang, D. Gray, D. Abbot, and X.-C. Zhang, "T-ray computed tomography," *Opt. Lett.*, vol. 27, no. 15, pp. 1312–1314, Aug. 2002.
[45] M. V. Duka, L. N. Dvoretskaya, N. S. Babelkin, M. K. Khodzitskii, S. A. Chivilikhin, and O. A. Smolyanskaya, "Numerical and experimental studies of mechanisms underlying the effect of pulsed broadband terahertz radiation on nerve cells," *Quantum Electron.*, vol. 44, no. 8, pp. 707–712, Aug. 2014.
[46] K. I. Zaytsev, K. G. Kudrin, V. E. Karasik, I. V. Reshetov, and S. O. Yurchenko, "*In vivo* terahertz spectroscopy of pigmentary skin nevi: Pilot study of non-invasive early diagnosis of dysplasia," *Appl. Phys. Lett.*, vol. 106, no. 5, Feb. 2015, Art. no. 053702.
[47] K. I. Zaytsev, A. A. Gavdush, N. V. Chernomyrdin, and S. O. Yurchenko, "Highly accurate *in vivo* terahertz spectroscopy of healthy skin: Variation of refractive index and absorption coefficient along the human body," *IEEE Trans. THz Sci. Technol.*, vol. 5, no. 5, pp. 817–827, Sep. 2015.
[48] K. I. Zaytsev, V. E. Karasik, I. N. Fokina, and V. I. Alekhnovich, "Invariant embedding technique for medium permittivity profile reconstruction using terahertz time-domain spectroscopy," *Opt. Eng.*, vol. 52, no. 6, Jun. 2013, Art. no. 068203.
[49] Z. J. Thompson, A. Stickel, Y.-G. Jeong, S. Han, B. H. Son, M. J. Paul, B. Lee, A. Mousavian, G. Seo, H.-T. Kim, Y.-S. Lee, and D.-S. Kim, "Terahertz-triggered phase transition and hysteresis narrowing in a nanoantenna patterned vanadium dioxide film," *Nano Lett.*, vol. 15, no. 9, pp. 5893–5898, Sep. 2015.
[50] B. Lee, A. Mousavian, M. J. Paul, Z. J. Thompson, A. D. Stickel, D. R. McCuen, E. Y. Jang, Y. H. Kim, J. Kyoung, D.-S. Kim, and Y.-S. Lee, "Anisotropic high-field terahertz response of free-standing carbon nanotubes," *Appl. Phys. Lett.*, vol. 108, no. 24, Jun. 2016, Art. no. 241111.
[51] M. J. Paul, B. Lee, J. L. Wardini, Z. J. Thompson, A. D. Stickel, A. Mousavian, H. Choi, E. D. Minot, and Y.-S. Lee, "Terahertz induced transparency in single-layer graphene," *Appl. Phys. Lett.*, vol. 105, no. 22, Dec. 2014, Art. no. 221107.
[52] P. Lopato, "Estimation of layered materials dielectric parameters using pulsed terahertz technique," *Int. J. Appl. Electromagn. Mech.*, vol. 43, nos. 1–2, pp. 161–168, Aug. 2013.
[53] K. Kawase, Y. Ogawa, Y. Watanabe, and H. Inoue, "Non-destructive terahertz imaging of illicit drugs using spectral fingerprints," *Opt. Exp.*, vol. 11, no. 20, pp. 2549–2554, Oct. 2003.
[54] J. Dong, A. Locquet, and D. S. Citrin, "Depth resolution enhancement of terahertz deconvolution by autoregressive spectral extrapolation," *Opt. Lett.*, vol. 42, no. 9, pp. 1828–1831, Apr. 2017.
[55] K. Su, Y.-C. Shen, and J. A. Zeitler, "Terahertz sensor for non-contact thickness and quality measurement of automobile paints of varying complexity," *IEEE Trans. THz Sci. Technol.*, vol. 4, no. 4, pp. 432–439, Jul. 2014.
[56] N. S. Balbekin, M. S. Kulya, P. Y. Rogov, and N. V. Petrov, "The modeling peculiarities of diffractive propagation of the broadband terahertz two-dimensional field," *Phys. Procedia*, vol. 73, pp. 49–53, Jan. 2015.
[57] N. V. Petrov, M. S. Kulya, A. N. Tsypkin, V. G. Bespalov, and A. Gorodetsky, "Application of terahertz pulse time-domain holography for phase imaging," *IEEE Trans. THz Sci. Technol.*, vol. 6, no. 3, pp. 464–472, May 2016.
[58] S. Gupta, V. Moroz, L. Smith, Q. Lu, and K. C. Saraswat, "7-nm FinFET CMOS design enabled by stress engineering using Si, Ge, and Sn," *IEEE Trans. Electron Devices*, vol. 61, no. 5, pp. 1222–1230, May 2014.
[59] M. Lapedus. *10 nm Versus 7 nm*. Accessed: Jan. 18, 2021. [Online]. Available: http://semiengineering.com/10nm-versus-7nm/
[60] M. S. Shur and J. Suarez, "Nanoscale silicon MOSFET response to THz radiation for testing VLSI," in *Proc. IEEE 27th North Atlantic Test Workshop (NATW)*, May 2018, pp. 1–6.
[61] M. Dyakonov and M. Shur, "Detection, mixing, and frequency multiplication of terahertz radiation by two-dimensional electronic fluid," *IEEE Trans. Electron Devices*, vol. 43, no. 3, pp. 380–387, Mar. 1996.
[62] W. Stillman, C. Donais, S. Rumyantsev, M. Shur, D. Veksler, C. Hobbs, C. Smith, G. Bersuker, W. Taylor, and R. Jammy, "Silicon FinFETs as detectors of terahertz and sub-terahertz radiation," *Int. J. High Speed Electron. Syst.*, vol. 20, no. 1, pp. 27–42, Mar. 2011.
[63] W. Stillman, F. Guarin, V. Y. Kachorovskii, N. Pala, S. Rumyantsev, M. S. Shur, and D. Veksler, "Nanometer scale complementary silicon MOSFETs as detectors of terahertz and sub-terahertz radiation," in *Proc. IEEE Sensors*, Oct. 2007, pp. 934–937.
[64] W. Stillman, M. S. Shur, D. Veksler, S. Rumyantsev, and F. Guarin, "Device loading effects on nonresonant detection of terahertz radiation by silicon MOSFETs," *Electron. Lett.*, vol. 43, no. 7, pp. 422–423, Mar. 2007.
[65] M. Shur and J. Suarez, "Terahertz testing of very large scale integrated circuits," in *Semiconductor Technology for Ultra Large Scale Integrated Circuits and Thin Film Transistors VII* (ECI Symposium Series), Y. Kuo, J. Murota, Y. Uraoka, and Y. Fukunaka, Eds. New York, NY, USA: ECI, 2019. Accessed: Jan. 18, 2021. [Online]. Available: https://dc.engconfintl.org/ ulsic_tft_vii/51
[66] M. Shur, S. Rudin, G. Rupper, M. Reed, and J. Suarez, "Sub-terahertz testing of millimeter wave monolithic and very large scale integrated circuits," *Solid-State Electron.*, vol. 155, pp. 44–48, May 2019.
[67] N. Akter, M. Karabiyik, A. Wright, M. Shur, and N. Pala, "AI powered THz testing technology for ensuring hardware cybersecurity," in *Proc. IEEE Res. Appl. Photon. Defense Conf. (RAPID)*, Aug. 2020, pp. 1–2.
[68] N. Akter, M. Karabiyik, M. Shur, J. Suarez, and N. Pala, "AI powered THz VLSI testing technology," in *Proc. IEEE 29th North Atlantic Test Workshop (NATW)*, Jun. 2020, pp. 1–5.
[69] G. Rupper, J. Suarez, S. Rudin, M. Reed, and M. Shur, "Terahertz plasmonics for testing very large-scale integrated circuits under bias," U.S. Patent US 10 890 618 B2, Jan. 12, 2021. Accessed: Jan. 18, 2021. [Online]. Available: https://patents.google.com/patent/US10890618B2/en
[70] M. S. Shur and J.-Q. Lu, "Terahertz sources and detectors using two-dimensional electronic fluid in high electron-mobility transistors," *IEEE Trans. Microw. Theory Techn.*, vol. 48, no. 4, pp. 750–756, Apr. 2000.
[71] X. Liu and M. Shur, "An efficient TCAD model for teraFET detectors operating in a large dynamic range," *IEEE Trans. THz Sci. Technol.*, vol. 10, no. 1, pp. 15–20, Jan. 2020.
[72] W. Stillman, D. Veksler, T. A. Elkhatib, K. Salama, F. Guarin, and M. S. Shur, "Sub-terahertz testing of silicon MOSFET," *Electron. Lett.*, vol. 44, no. 22, pp. 1325–1327, Oct. 2008.
[73] C. Eakins, B. Dupaix, and R. Ott, "Assessment of required minimum sample size in variation signature based approaches to device authentication," in *Proc. Government Microcircuit Appl. Crit. Technol. Conf. (GOMACTech)*, 2018, pp. 4–9.
[74] S. K. Moore, "X-ray tech lays chip secrets bare," *IEEE Spectr., Nanoclast Blog, Semicond. Designs Sect.*, Oct. 2019. Accessed: Jan. 18, 2021. [Online]. Available: https://spectrum.ieee.org/nanoclast/semiconductors/design/xray-tech-lays-chip-secrets-bare

[75] J. Deng, Y. P. Hong, S. Chen, Y. S. G. Nashed, T. Peterka, A. J. F. Levi, J. Damoulakis, S. Saha, T. Eiles, and C. Jacobsen, ''Nanoscale X-ray imaging of circuit features without wafer etching,'' *Phys. Rev. B, Condens. Matter*, vol. 95, no. 10, Mar. 2017, Art. no. 104111.

[76] S. L. Rumyantsev, A. Muraviev, S. Rudin, G. Rupper, M. Reed, J. Suarez, and M. Shur, ''Terahertz beam testing of millimeter wave monolithic integrated circuits,'' *IEEE Sensors J.*, vol. 17, no. 17, pp. 5487–5491, Sep. 2017.

[77] T. A. Elkhatib, A. V. Muravjov, D. B. Veksler, W. J. Stillman, X-C. Zhang, M. S. Shur, and V. Y. Kachorovskii, ''Subwavelength detection of terahertz radiation using GaAs HEMTs,'' in *Proc. IEEE Sensors*, Oct. 2008, pp. 1988–1990.

NAZNIN AKTER received the B.Sc. (Hons.) and M.S. degrees in applied physics, electronics, and communication engineering from the University of Dhaka, Bangladesh, in 2012 and 2014, respectively, and the master's degree from the Department of Electrical and Computer Engineering (ECE), Florida International University (FIU), Miami, FL, USA. She is currently pursuing the Ph.D. degree with the INSYST Integrated Nanosystems Research Lab, Department of Electrical and Computer Engineering, FIU. Her research interests include simulation, fabrication, and characterization of micro and nanostructured THz emitters and detectors.

MASUDUR R. SIDDIQUEE received the bachelor's and M.S. degrees from the Department of Applied Physics, Electronics and Communication Engineering, University of Dhaka, in 2009 and 2011, respectively, and the M.S. and Ph.D. degrees from the Department of Electrical and Computer Engineering (ECE), Florida International University (FIU), Miami, FI, USA, in 2019 and 2020, respectively. Afterward, he worked in the telecommunication industry as a Core Network Engineer for four and a half years. He worked with the Human Cyber-Physical Systems (HCPS) Laboratory, FIU. He is currently a Postdoctoral Associate with the Applied Research Center (ARC), FIU. During his tenure in HCPS, he was involved in the research and development of human body area sensor systems, such as fNIRS, ECG, and EMG. His research interest includes human mental state estimation using non-invasive sensing modalities during gait.

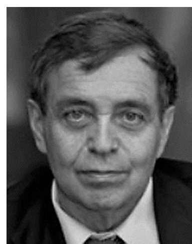

MICHAEL SHUR (Life Fellow, IEEE) received the M.S.E.E. degree (Hons.) from the St. Petersburg Electrotechnical Institute, Russia, in 1965, and the Ph.D. degree in physics and the D.Sc. (Habilitation) degree in physics and mathematics from the A. F. Ioffe Institute of Physics and Technology, St. Petersburg, Russia, in 1967 and 1992, respectively. He is currently a Patricia W. and C. Sheldon Roberts Professor with the Solid-State Electronics Rensselaer Polytechnic Institute, Troy, NY, USA. He is also the CTO of Electronics of the Future, Inc. He holds many patents on solid state devices and authored many technical articles and books, including books on GaAs, GaN devices and circuits, physics of semiconductor devices, and an undergraduate text on electronic devices. His research interests include ferroelectrics, amorphous semiconductors, solar cells, ballistic transport, high-speed semiconductor devices, and integrated circuits. In 1994, he was awarded an Honorary Doctorate by the St. Petersburg State Technical University.

NEZIH PALA (Senior Member, IEEE) received the M.S. and Ph.D. degrees in electrical engineering from the Rensselaer Polytechnic Institute, Troy, NY, USA, in 1999 and 2002, respectively. He is currently an Associate Professor with the Department of Electrical and Computer Engineering, Florida International University. He has authored/coauthored more than 150 articles published in peer-reviewed scientific journals and conferences. His research interests include the design, fabrication, and characterization of nanoscale electronic and photonic devices and systems for sensing, imaging, communication, and energy harvesting.